# Crystal structure and thermoelectric properties of KxBa8−xZnyGe46−y clathrates

Kengo Kishimoto, Yuta Sasaki, Tsuyoshi Koyanagi, Kenji Ohoyama, and Koji Akai

## Related Articles

Atomistic calculation of the local structure in bulk and strained semiconductor alloys
J. Appl. Phys. 112, 113515 (2012)

Second-order many-body perturbation study of ice Ih
J. Chem. Phys. 137, 204505 (2012)

Effect of high-pressure on the electronic and magnetic properties in double perovskite oxide Sr2FeMoO6
J. Appl. Phys. 112, 103712 (2012)

Crystal structure and epitaxy of Bi2Te3 films grown on Si
Appl. Phys. Lett. 101, 221910 (2012)

Giant stability of substituent Co chains in ZnO:Co dilute magnetic oxides
AIP Advances 2, 042155 (2012)

## Additional information on J. Appl. Phys.

Journal Homepage: http://jap.aip.org/

Journal Information: http://jap.aip.org/about/about_the_journal

Top downloads: http://jap.aip.org/features/most_downloaded

Information for Authors: http://jap.aip.org/authors

# Crystal structure and thermoelectric properties of $K_xBa_{8-x}Zn_yGe_{46-y}$ clathrates

Kengo Kishimoto,[1,a)] Yuta Sasaki,[1] Tsuyoshi Koyanagi,[1] Kenji Ohoyama,[2] and Koji Akai[3]

[1]*Graduate School of Science and Engineering, Yamaguchi University, 2-16-1 Tokiwadai, Ube, Yamaguchi 755-8611, Japan*
[2]*Institute for Materials Research, Tohoku University, 2-1-1 Katahira, Sendai 980-8577, Japan*
[3]*Media and Information Technology Center, Yamaguchi University, 1677-1 Yoshida, Yamaguchi 753-8511, Japan*

Polycrystalline samples of degenerate *n*-type $K_xBa_{8-x}Zn_yGe_{46-y}$ ($y \sim 8 - x/2$) with the type-I clathrate structure (No. 223, $Pm\bar{3}n$) were prepared by powder metallurgy to obtain a high-efficiency Ge-based clathrate. Their Zn atoms preferred to exist at the $6c$ site in the framework, and consequently, the samples with $x$ around 4, such as $K_4Ba_4Zn_6Ge_{40}$, possessed highly ordered Zn/Ge atom frameworks whose $6c$, $16i$, and $24k$ sites were occupied almost solely by Zn, Ge, and Ge atoms, respectively. In spite of such ordered structures and small numbers of substituting Zn atoms, these samples exhibited carrier mobilities lower than those of $Ba_8Zn_8Ge_{38}$ and $Ba_8Ga_{16}Ge_{30}$. Band structure calculations implied that the combination of the rattler K and Ba atoms in the cages considerably modified the conduction band edge of the corresponding clathrates; such a modification is considered to strengthen alloy disorder scattering, which reduces carrier mobility. The maximum dimensionless figure-of-merit $ZT$ was 0.51 at 1000 K for the $K_2Ba_6Zn_7Ge_{39}$ sample, which is similar to that of 0.50 at 900 K for the $Ba_8Zn_8Ge_{38}$ sample. © 2012 American Institute of Physics. [http://dx.doi.org/10.1063/1.4711100]

## I. INTRODUCTION

Thermoelectric materials can be used for the conversion of waste heat to electricity, which is expected to be an energy-saving technology. Researchers in the thermoelectric community have therefore been developing high-efficiency thermoelectric materials. The dimensionless figure-of-merit $ZT$ is expressed approximately by

$$ZT \propto \frac{m^{*3/2}\mu}{\kappa_L}T,\qquad(1)$$

where $m^*$ is the effective mass, $\mu$ is the mobility, $\kappa_L$ is the lattice thermal conductivity, and $T$ is the absolute temperature.[1] Semiconducting clathrate compounds of group IV elements are good thermoelectric materials because of their very low $\kappa_L$ value as a result of the "rattling" motion of the atoms filling in their cages.[2–6] Such clathrates also have the advantage that they can be produced using non-toxic elements. To date, several Ge- and Si-based compounds with the type-I clathrate structure (No. 223, $Pm\bar{3}n$) have been reported to possess $ZT$ values of approximately 1 at elevated temperatures;[2,3,7–9] the maximum $ZT$ values of single-crystal and polycrystalline samples are 1.35 at 900 K for $Ba_8Ga_{16}Ge_{30}$ (Ref. 7) and 1.2 at 1000 K for $Ba_8Ni_{0.31}Zn_{0.52}Ga_{13.06}Ge_{32.2}$ (Ref. 8).

Equation (1) indicates that a higher carrier mobility $\mu$ results in a larger $ZT$ value. Carrier conduction in semiconducting clathrates is considered to suffer from alloy disorder scattering and ionized impurity scattering, as well as acoustic phonon scattering. Figure 1 shows the crystal structure of the type-I clathrate $Ba_8(X,Ge)_{46}$, where X represents an element such as Ga or Zn which substitutes for Ge in the framework, and the X atom compensates for excess electrons provided by Ba. The X atoms may reduce carrier mobility by alloy disorder scattering and/or ionized impurity scattering. So, a decrease in the number of the X atoms may increase the carrier mobility in the clathrate. The following room-temperature (RT) mobilities larger than that of approximately 10 $cm^2$ $V^{-1}$ $s^{-1}$ for $Ba_8Ga_{16}Ge_{30}$ (Refs. 3, 11, and 12) have been obtained: 21, 18, and 17 $cm^2$ $V^{-1}$ $s^{-1}$ for $Ba_{8.11}Cu_{4.12}Ga_{4.06}Ge_{37.71}$ (Ref. 13), $Ba_8Zn_{7.83}Ge_{38.17}$ (Ref. 14), and $Ba_8Ni_{2.97}Zn_{3.94}Ge_{39.09}$ (Ref. 8), respectively. However, these differences are associated with decreases not only in the number of substituting atoms but also in the effective mass $m^*$. Consequently, the corresponding weighted mobilities $m^{*3/2}\mu$, as well as the resultant $ZT$ increased to a small degree.

The substitution of alkali metals such as K for the Ba atoms filling in the cages can also reduce the number of X atoms in the framework. In a previous paper, we reported that the type-I clathrate $K_8Ga_8Sn_{38}$ has a higher mobility and $ZT$ value than that of the type-I clathrate $Ba_8Ga_{16}Sn_{30}$ (Ref. 15). We also prepared sintered samples of $K_xBa_{8-x}Ga_yGe_{46-y}$ in another study.[17] Xie synthesized a $K_8Zn_4Ge_{42}$ clathrate;[16] the thermoelectric properties have not been reported.

Apart from the above-mentioned reduction in the number of X atoms, ordering of the X/Ge atom configuration in the framework possibly raises the carrier mobility because of the suppression of alloy disorder scattering. Metal atoms such as Ni, Cu, and Zn prefer to occupy the $6c$ sites in the framework (Fig. 1).[18–26] $Ba_8M_6Ge_{40}$ clathrates substituted with such metal elements M are therefore expected to have ordered
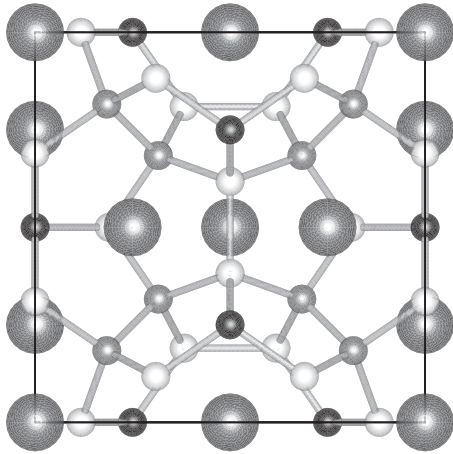
FIG. 1. Crystal structure of the type-I clathrate $Ba_8(X,Ge)_{46}$. Large balls represent Ba atoms and smaller balls represent X and Ge atoms; black, gray, and white balls are at the $6c$, $16i$, and $24k$ sites, respectively. This figure was drawn using the VESTA program (Ref. [10]).

structures. Hokazono *et al.* discussed the effects of such ordering on the mobility of some $Ba_8Cu_xGa_{16-3x}Ge_{30+2x}$ ($0 \leq x \leq 5$) samples,[13] where the observed increases in mobility were mainly as a result of a decrease in the number of substituting atoms. Johnsen *et al.* characterized several $Ba_8Ni_{6-x}Ge_{40+x}$ ($0 \leq x \leq 0.6$) samples.[20] However, disappointingly, they did not obtain increases in carrier mobility, which is possibly attributable to the existence of vacancies in their frameworks. Melnychenko-Koblyuk *et al.* and Koza *et al.* prepared ternary Ba-Zn-Ge clathrates.[21,24] The $Ba_8Zn_xGe_y$ ($0 \leq x \leq 6$) samples contained vacancies in their frameworks, which probably scattered carrier electrons and reduced carrier mobility. On the other hand, Nasir *et al.* prepared vacancy-free quaternary clathrates $Ba_8(Zn,Cu)_6Ge_{40}$ and $Ba_8(Zn,Pd)_6Ge_{40}$, whose $6c$ sites were occupied almost solely by Zn and Cu or Pd atoms; unfortunately, these clathrates are not reported to have high $ZT$ values.[25] Since the Zn and Cu or Pd atoms were present randomly at the $6c$ sites in the frameworks,[25] this randomness might suppress increases in carrier mobility.

In this study, we prepared $K_xBa_{8-x}Zn_yGe_{46-y}$ clathrates to investigate their crystal structures, transport properties, and thermoelectric properties. We anticipated that the $K_4Ba_4Zn_6Ge_{40}$ clathrate would possess an ordered framework with $6c$, $16i$, and $24k$ sites occupied solely by Zn, Ge, and Ge atoms, respectively. We were also interested in the properties of the $K_8Zn_4Ge_{42}$ clathrate mentioned above.

## II. EXPERIMENTAL

Nominal $K_xBa_{8-x}Zn_yGe_{46-y}$ polycrystalline samples were obtained as follows. The starting materials were K (99%), Ba (99.9%), Zn (99.999%), and Ge (99.9999%); they were weighed to a composition ratio of $K_{1.1x}Ba_{1.03(8-x)}Zn_yGe_{46-y}$, with excess of K and Ba of 10 and 3 wt. %, respectively, to compensate for their mass losses during sample preparation. K, Zn, and an arc-melted Ba-Ge alloy were placed in BN-coated Nb crucibles, which were sealed inside stainless-steel containers under Ar. The containers were heated and kept at 1223 K for 24 h in an Ar flow. The resulting materials were ground to fine powders (below $100\,\mu m$), which were then sintered by spark plasma sintering (SPS) with graphite

dies. Sintering was performed at 1058–1113 K for 30 min under 40 MPa in standing Ar at 0.5 atm. For comparison, a $Ba_8Ga_{16}Ge_{30}$ sample was produced from a powder of arc-melted Ba-Ga-Ge alloy using the SPS method.

The crystal structures of the samples were examined using powder x-ray diffraction (XRD) and powder neutron diffraction (ND) at RT; the ND measurements were performed with the high-efficiency and high-resolution diffractometer, HERMES, of the Institute for Materials Research (IMR), Tohoku University, installed at the JRR-3 reactor at the Japan Atomic Energy Agency (JAEA).[27] The Rietveld analyses were performed using the Rietveld analysis program RIETAN-FP,[28] which provided the structural parameters as well as the weight percentages of the secondary phases contained in the samples. The chemical compositions of the samples were determined using electron probe microanalysis (EPMA) with an energy dispersive Horiba EMAX-7000. Sample densities $\rho$ were determined by the Archimedes method. Electrical conductivities $\sigma$ were measured using the four-probe method. The Seebeck coefficients $S$ were measured using the steady-state method. The electrical conductivities and Seebeck coefficients were measured at 100–1000 K in a vacuum. Thermal conductivities $\kappa$ were obtained at 300–1000 K using the relation $\kappa = \alpha C \rho$; the thermal diffusivities $\alpha$ were measured in a vacuum using the laser flash method and specific heats $C$ were calculated using the Dulong-Petit law ($C_{DP}$). Hall measurements were carried out at 100–300 K; carrier concentrations $n$ were determined from the relation $n = 1/(eR_H)$, where $e$ is the electronic charge and $R_H$ is the Hall coefficient. Hall mobilities $\mu_H$ were calculated from the relation $\mu_H = \sigma R_H$.

The RT effective masses $m^*$ were estimated using a single parabolic band model with a scattering factor $r$ of $-1/2$. In this model, $S$ and $n$ are given by $S = -(k/e)\{2F_1(\eta^*)/F_0(\eta^*) - \eta^*\}$ and $n = 4\pi(2m^*kT/h^2)^{3/2}F_{1/2}(\eta^*)$, respectively, where $k$ is the Boltzmann constant, $\eta^*$ is the reduced Fermi energy, $F_t$ is a Fermi integral of order $t$, and $h$ is Planck's constant.[1] $\eta^*$ was calculated from $S$, using the former equation, and then $m^*$ was calculated from $\eta^*$ and $n$ using the latter equation. The lattice thermal conductivities $\kappa_L$ were estimated using $\kappa_L = \kappa - L\sigma T$, where the Lorenz number $L$ is given by $(k/e)^2\{3F_2(\eta^*)/F_0(\eta^*) - 4F_1^2(\eta^*)/F_0^2(\eta^*)\}$.[1]

The electronic structures of $K_8Zn_4Ge_{42}$ and $Ba_8Zn_8Ge_{38}$ were calculated using a full-potential augmented plane-wave method with a generalized gradient approximation.[29,30]

## III. RESULTS AND DISCUSSION

### A. Crystal structures

Figure 2 shows the powder ND pattern of the nominal $K_4Ba_4Zn_6Ge_{40}$ sample and the powder XRD pattern of the nominal $K_8Zn_4Ge_{42}$ sample. The obtained $K_xBa_{8-x}Zn_yGe_{46-y}$ samples almost exhibited a single phase of a type-I clathrate structure (No. 223, $Pm\bar{3}n$); they included Ge ($Fd\bar{3}m$, No. 227), $Ba_6Ge_{25}$ ($P4_132$, No. 213), and $BaZn_2Ge_2$ ($I4/mmm$, No. 139) as secondary impurity phases, where the total weight percentage of the impurity phases was less than 2 wt. %.

Table I lists the structural parameters for the $K_xBa_{8-x}Zn_{8-x/2}Ge_{38+x/2}$ clathrate samples, refined by the
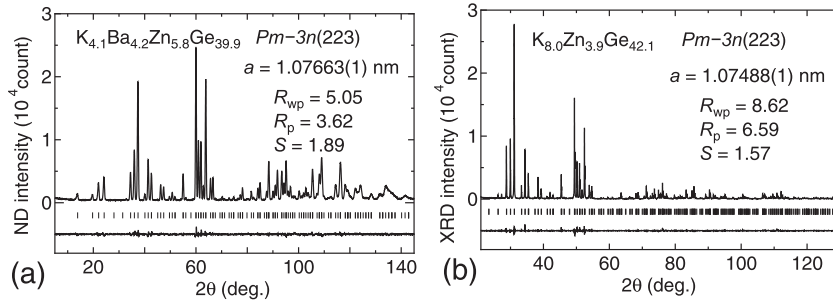
FIG. 2. (a) Powder neutron diffraction pattern of the $K_4Ba_4Zn_6Ge_{40}$ sample and (b) powder x-ray diffraction pattern of the $K_8Zn_4Ge_{42}$ sample, refined by Rietveld analysis.

Rietveld method under the condition that no vacancy existed at each site. We used the split-site model for the rattler K/Ba atoms in the larger (or tetradodecahedral) cages in the type-I clathrate,[31,32] where the $24j$ split-site model resulted in a slightly better fit than the $24k$ model did.[22] The obtained data for $K_8Zn_4Ge_{42}$ are almost equal to the data previously reported,[16] and the data for $Ba_8Zn_8Ge_{38}$ are roughly the same as those previously reported.[21,22] As did in the previous studies,[21–24] this study revealed that the Zn atoms preferred to exist at the $6c$ sites. Unfortunately, we could not synthesize a sample with a perfectly ordered Zn/Ge framework whose $6c$, $16i$, and $24k$ sites were occupied solely by Zn, Ge, and Ge atoms, respectively, although the $K_2Ba_6Zn_7Ge_{39}$ and $K_4Ba_4Zn_6Ge_{40}$ samples seem to possess highly ordered Zn/Ge frameworks. The Rietveld analysis also indicated that the K atoms, being larger than Ba, preferred to exist at the $24j$ sites, which are wider than the $2a$ sites, and that the samples with higher K contents had larger equivalent atomic displacement parameters $U_{eq}$, as well as smaller split distances

$d = |y(24j) - 1/2|$ for the rattler K/Ba atoms. We will discuss their influences on the thermal conductivity later.

## B. Mobility and effective mass

Table II lists RT primary properties for the $K_xBa_{8-x}Zn_yGe_{46-y}$ clathrate samples. The carrier concentrations $n$ were of the order $10^{20}$ cm$^{-3}$. One carrier per unit cell equals $1/a^3 \sim 8 \times 10^{20}$ cm$^{-3}$. Carrier compensation was therefore roughly complete in the obtained samples. We anticipated increases in the carrier mobility $\mu$ for the K-containing samples, but these samples, including the ones with highly ordered frameworks, exhibited reduced carrier mobility. Consequently, we could obtain no increase in the materials factor $\beta = (m^*/m_e)^{3/2}\mu_H/\kappa_L$, although some increases in the weighted mobility $U_H = (m^*/m_e)^{3/2}\mu_H$ were achieved.

We think that the reductions in the carrier mobility $\mu$ may be associated with increases in the effective mass $m^*$ for

TABLE I. Structural parameters for the $K_xBa_{8-x}Zn_{8-x/2}Ge_{38+x/2}$ clathrate (No. 223, $Pm\bar{3}n$) samples, refined by the Rietveld method using powder neutron and x-ray diffraction under the following conditions: (1) no vacancy exists; (2) K and Ba atoms occupy $2a$ (0, 0, 0) and $24j$ (1/4, y, 1/2 + y) sites, and Zn and Ge atoms occupy $6c$ (1/4, 0, 1/2), $16i$ (x, x, x), and $24k$ (0, y, z) sites; (3) both the K/Ba and Zn/Ge ratios are the same as those determined by electron probe microanalysis; (4) equivalent atomic displacement parameters $U_{eq}$ are equal at each site.

| Parameter | $Ba_8Zn_8Ge_{38}$ | $K_2Ba_6Zn_7Ge_{39}$ | $K_4Ba_4Zn_6Ge_{40}$ | $K_6Ba_2Zn_5Ge_{41}$ | $K_8Zn_4Ge_{42}$[a] |
|---|---|---|---|---|---|
| EPMA[b] | $Ba_{8.4}Zn_{8.0}Ge_{37.7}$ | $K_{1.9}Ba_{6.6}Zn_{6.9}Ge_{38.7}$ | $K_{4.1}Ba_{4.2}Zn_{5.8}Ge_{39.9}$ | $K_{6.2}Ba_{2.2}Zn_{5.0}Ge_{40.6}$ | $K_{8.0}Zn_{3.9}Ge_{42.1}$ |
| $a$ (nm)[c] | 1.07670(1) | 1.07653(1) | 1.07663(1) | 1.07658(2) | 1.07488(1) |
| $R_{wp}, R_p$ | 4.48, 3.37 | 4.92, 3.58 | 5.05, 3.62 | 4.54, 3.29 | 8.62, 6.59 |
| $S = R_{wp}/R_e$ | 1.59 | 1.82 | 1.89 | 1.70 | 1.57 |
| $g$ (K, $2a$) | 0 | 0.035 | 0.149 | 0.375 | 1 |
| $g$ (K, $24j$) | 0 | 0.072(1) | 0.153(1) | 0.215(1) | 1/4 |
| $g$ (Zn, $6c$) | 0.88(1) | 0.95(1) | 0.93(1) | 0.80(1) | |
| $g$ (Zn, $16i$) | 0.05(1) | 0.04(1) | 0.01(1) | 0.01(1) | |
| $g$ (Zn, $24k$) | 0.09 | 0.03 | 0.00 | 0.00 | |
| $y$ ($24j$) | 0.5153(4) | 0.511(1) | 0.510(1) | 0.509(1) | 0.512(1) |
| $x$ ($16i$) | 0.18365(6) | 0.18352(7) | 0.18332(7) | 0.18323(6) | 0.18333(7) |
| $y$ ($24k$) | 0.30946(6) | 0.30955(6) | 0.30952(6) | 0.30935(5) | 0.3086(1) |
| $z$ ($24k$) | 0.11761(6) | 0.11721(6) | 0.11708(6) | 0.11735(5) | 0.1174(1) |
| $U_{eq}$ ($2a$) (Å$^2$) | 0.005(1) | 0.004(1) | 0.002(1) | 0.003(1) | 0.012(3) |
| $U_{eq}$ ($24j$) (Å$^2$) | 0.019(1) | 0.025(1) | 0.026(2) | 0.030(2) | 0.027(4) |
| $U_{eq}$ ($6c$) (Å$^2$) | 0.0085(6) | 0.0084(7) | 0.0089(7) | 0.0085(6) | 0.009(2) |
| $U_{eq}$ ($16i$) (Å$^2$) | 0.0091(2) | 0.0081(3) | 0.0079(3) | 0.0078(2) | 0.008(2) |
| $U_{eq}$ ($24k$) (Å$^2$) | 0.0100(2) | 0.0090(2) | 0.0088(2) | 0.0090(2) | 0.008(2) |
| $W$ (wt. %)[d] | 0.0, 0.0, 0.0 | 0.4, 0.5, 0.2 | 0.5, 0.9, 0.1 | 1.0, 0.7, 0.2 | 1.3, 0.0, 0.0 |

[a]Neutron diffraction was not measured for the $K_8Zn_4Ge_{42}$ sample.
[b]Chemical composition determined by EPMA.
[c]Lattice constant.
[d]Weight percentage of impurity phases. The first, second, and third values are for Ge, $Ba_6Ge_{25}$ and $BaZn_2Ge_2$, respectively.

TABLE II. Room-temperature properties of the $K_xBa_{8-x}Zn_yGe_{46-y}$ clathrate samples: $\rho$ (g/cm$^3$), density; $n$ ($10^{20}$ cm$^{-3}$), carrier concentration; $\mu_H$ (cm$^2$ V$^{-1}$ s$^{-1}$), Hall mobility; $m^*$ ($m_e$), effective mass; $U_H = (m^*/m_e)^{3/2}\mu_H$ (cm$^2$ V$^{-1}$ s$^{-1}$), weighted mobility; $\kappa_L$ (mW cm$^{-1}$ K$^{-1}$), lattice thermal conductivity; $\beta = (m^*/m_e)^{3/2}\mu_H/\kappa_L$ ($10^3$ cm$^3$ K V$^{-1}$ J$^{-1}$), materials factor.

| Sample[a] | $\rho$ | $n$ | $\mu_H$ | $m^*$ | $U_H$ | $\kappa_L$ | $\beta$ |
|---|---|---|---|---|---|---|---|
| $Ba_8Zn_8Ge_{38}$ | 5.794 | 4.9 | 17 | 1.1 | 20 | 13 | 1.6 |
| $K_2Ba_6Zn_7Ge_{39}$ | 5.542 | 6.9 | 12.4 | 1.3 | 19 | 16 | 1.2 |
| $K_3Ba_5Zn_6Ge_{40}$ | | 9.5 | 9.4 | 1.9 | 24 | 21 | 1.2 |
| $K_4Ba_4Zn_6Ge_{40}$ | 5.267 | 2.2 | 7.3 | 1.7 | 16 | 18 | 0.9 |
| $K_6Ba_2Zn_5Ge_{41}$ | 5.048 | 2.4 | 1.7 | 4.7 | 18 | 21 | 0.8 |
| $K_8Zn_4Ge_{42}$ | 4.676 | 6.0 | 3.0 | 5.0 | 34 | 29 | 1.2 |
| $Ba_8Ga_{16}Ge_{30}$ | 5.791 | 3.2 | 15.3 | 1.5 | 28 | 12 | 2.2 |

[a]The chemical formulas indicate sample nominal composition.

the K-containing samples because the effective mass $m^*$ increased with the K content. Figure 3 plots the band structures and densities-of-state (DOS) for the $Ba_8Zn_8Ge_{38}$ and $K_8Zn_4Ge_{42}$ clathrates. The band structure calculation was carried out in the virtual crystal approximation using the structural parameters listed in Table I, except that the rattler K/Ba atoms were set to exist at the $6d(1/4, 1/2, 0)$ site instead of the $24j(1/4, y, 1/2 + y)$ site.[33] Both the conduction band minima are present at the M point. In a previous paper,[34] we demonstrated that the conduction band minimum of $Ba_8Zn_8Ge_{38}$ is of lower energy than that of $Ba_8Ga_{16}Ge_{30}$, which causes band gap narrowing as well as a decrease in
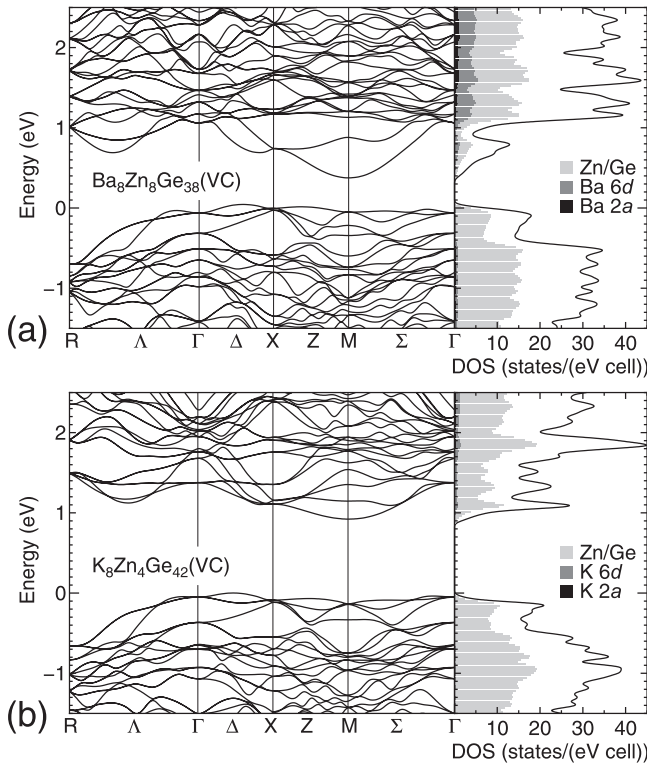


FIG. 3. Band structures and densities-of-state for (a) $Ba_8Zn_8Ge_{38}$ and (b) $K_8Zn_4Ge_{42}$ clathrates calculated in the virtual crystal approximation. The solid curve in the right-hand side of the figure indicates the total DOS, and the black, dark gray, and light gray areas indicate partial DOSs of the K/Ba atoms at the 2a site, of the K/Ba atoms at the 6d site, and of all the Zn/Ge atoms, respectively.
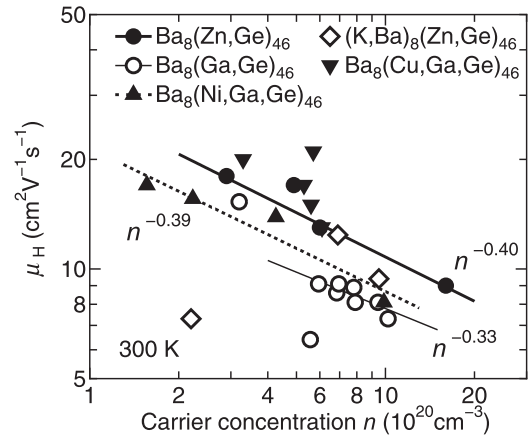


FIG. 4. Room-temperature Hall mobility $\mu_H$ as a function of carrier concentration $n$ for the $K_xBa_{8-x}Zn_yGe_{46-y}$ samples and some related clathrates: $Ba_8(Zn,Ge)_{46}$ (Ref. 14), $Ba_8(Ga,Ge)_{46}$ (Ref. 11), $Ba_8(Ni,Ga,Ge)_{46}$ (Ref. 8), and $Ba_8(Cu,Ga,Ge)_{46}$ (Ref. 13). The lines fit $\mu_H \propto n^t$ (t: constant).

the effective mass. In contrast, the conduction band minimum of $K_8Zn_4Ge_{42}$ increases in energy, which results in a band gap increase as well as an increase in the effective mass. The difference between these conduction bands is caused by the difference between the orbitals of the rattler K and Ba atoms: as seen in Fig. 3, the conduction band edge of $Ba_8Zn_8Ge_{38}$ has a pronounced Ba orbital character,[34] whereas that of $K_8Zn_4Ge_{42}$ has virtually no K orbital character. We therefore concluded that the measured mobilities, as well as the effective masses mentioned above, were affected by changes in the band structures of the K-containing clathrates.

Figure 4 plots the RT Hall mobility $\mu_H$ as a function of carrier concentration $n$ for the $K_x Ba_{8-x}Zn_yGe_{46-y}$ samples and some related clathrates $Ba_8(Zn,Ge)_{46}$ (Ref. 14), $Ba_8(Ga,Ge)_{46}$ (Ref. 11), $Ba_8(Ni,Ga,Ge)_{46}$ (Ref. 8), and $Ba_8(Cu,Ga,Ge)_{46}$ (Ref. 13). The three lines fit $\mu_H \propto n^t$ (t: constant). The relation $\mu \propto n^{-1/3}$ is observed for a degenerate semiconductor whose carrier mobility is controlled by acoustic phonon scattering.[20,35] The $Ba_8(Zn,Ge)_{46}$, $Ba_8(Ga,Ge)_{46}$, and $Ba_8(Ni,Ga,Ge)_{46}$ clathrates almost obey this relation,
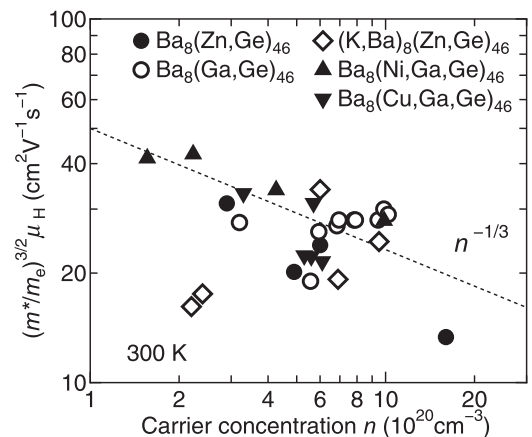


FIG. 5. Room-temperature weighted mobility $(m^*/m_e)^{3/2}\mu_H$ as a function of carrier concentration $n$ for $K_xBa_{8-x}Zn_yGe_{46-y}$ and some Ba-containing Ge clathrates (Refs. 8, 11, 13, and 14). The line $\mu_H \propto n^{-1/3}$ is a guide for the eyes.
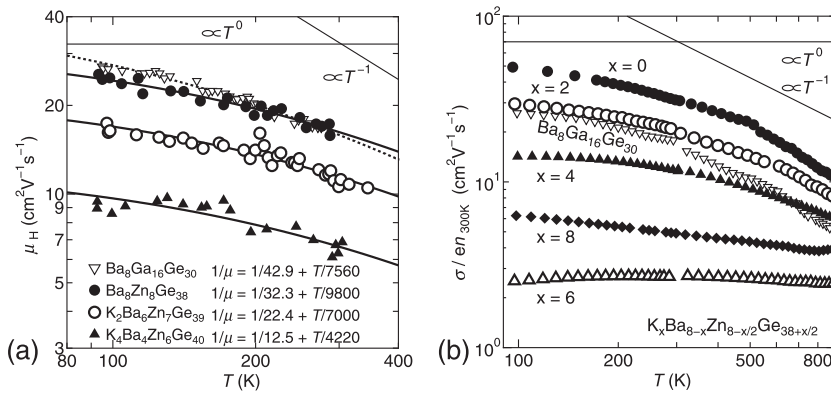
FIG. 6. Temperature dependences of (a) Hall mobility $\mu_H$ and (b) the $\sigma/(en_{300K})$ value for the $K_xBa_{8-x}Zn_{8-x/2}Ge_{38+x/2}$ and $Ba_8Ga_{16}Ge_{30}$ samples. The thin lines in proportion to $T^0$ and $T^{-1}$ represent the temperature dependences of mobilities dominated by alloy disorder scattering and acoustic phonon scattering, respectively. The thick solid and dotted curves fit the relation $1/\mu_H = 1/M1 + T/M2$ ($M1$, $M2$: constant).

whereas the $(K,Ba)_8(Zn,Ge)_{46}$ and $Ba_8(Cu,Ga,Ge)_{46}$ clathrates do not obey it, because of the substantial changes in the effective mass.

Some of the mobilities of the $K_xBa_{8-x}Zn_yGe_{46-y}$ samples were larger than those of $Ba_8Ga_{16}Ge_{30}$; however, they did not exceed those of the related clathrates. Figure 5 plots the RT weighted mobility $(m^*/m_e)^{3/2}\mu_H$ as a function of carrier concentration $n$ for the $K_xBa_{8-x}Zn_yGe_{46-y}$ samples and some related clathrates.[8,11,13,14] The weighted mobilities of the $K_xBa_{8-x}Zn_yGe_{46-y}$ samples were not as large as those of the related clathrates, but the $K_8Zn_4Ge_{42}$ sample showed a relatively large value as a result of its larger effective mass. To sum up so far, we could not obtain increases in mobility and in weighted mobility for $K_xBa_{8-x}Zn_yGe_{46-y}$, including $K_4Ba_4Zn_6Ge_{40}$ with a highly ordered framework.

We further examined the carrier mobilities of the $K_xBa_{8-x}Zn_yGe_{46-y}$ samples. Figure 6(a) shows the temperature dependences of the Hall mobilities $\mu_H$ at low temperatures for the $K_xBa_{8-x}Zn_{8-x/2}Ge_{38+x/2}$ samples with $x = 0$, 2, and 4. Since we could not determine the Hall voltage for the samples with $x = 6$ and 8 because of electrical noise, we plotted the $\sigma/(en_{300K})$ values in Fig. 6(b), where $n_{300K}$ is the carrier concentration at 300 K. For comparison, the data for the $Ba_8Ga_{16}Ge_{30}$ sample are also plotted. As indicated by the thick curves, the data in Fig. 6(a) can be well fitted to the relation

$$\frac{1}{\mu} = \frac{1}{\mu_1} + \frac{1}{\mu_2} = \frac{1}{M1} + \frac{T}{M2}, \tag{2}$$

which is based on Matthiessen's rule, where $M1$ and $M2$ are constants. The calculated fitting parameters are as follows: ($M1$ (cm$^2$ V$^{-1}$ s$^{-1}$), $M2$ (cm$^2$ V$^{-1}$ s$^{-1}$ K)) = (32.3, 9800), (22.4, 7000), (12.5, 4220), and (42.9, 7560) for the $Ba_8Zn_8Ge_{38}$, $K_2Ba_6Zn_7Ge_{39}$, $K_4Ba_4Zn_6Ge_{40}$, and $Ba_8Ga_{16}Ge_{30}$ samples, respectively.

The temperature dependences of carrier mobilities $\mu_{ac}$, $\mu_{al}$, and $\mu_i$, dominated by acoustic phonon scattering, alloy disorder scattering, and ionized impurity scattering, respectively, are given as follows:

$$\mu_{ac} \propto \frac{T^{-1}}{m^{*5/2}}, \tag{3}$$

$$\mu_{al} \propto \frac{T^0}{m^{*5/2}}, \tag{4}$$

$$\mu_i \propto \frac{T^0}{m^{*1/2}N_i}, \tag{5}$$

where $N_i$ is the number of ionized impurity atoms. Since the positions of the conduction band minima in the $k$-space for the clathrates examined do not differ from each other, in this paper, we simply use the effective mass $m^*$ instead of the DOS effective mass and conductivity effective mass. If ionized impurity scattering was dominant at lower temperatures, the $K_4Ba_4Zn_6Ge_{40}$ sample with a smaller carrier concentration would have possessed a higher mobility. However, this was not true for our samples. We therefore believe that the dominant scattering at lower temperatures was alloy disorder scattering, whereas that at higher temperatures was acoustic
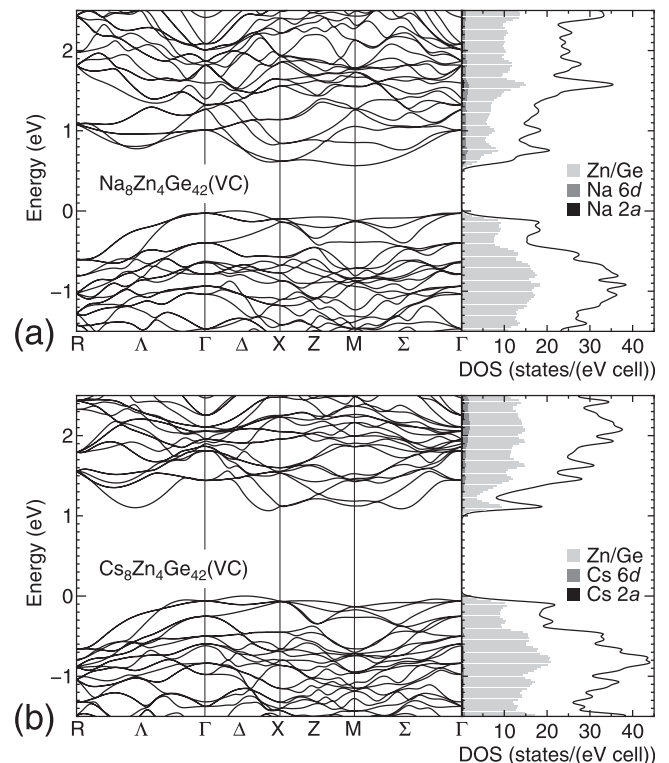


FIG. 7. Band structures and densities-of-state for hypothetical (a) $Na_8Zn_4Ge_{42}$ and (b) $Cs_8Zn_4Ge_{42}$ clathrates calculated in the virtual crystal approximation. The solid curve in the right-hand side of the figure indicates the total DOS, and the black, dark gray, and light gray areas indicate partial DOSs of the Na/Cs atoms at the $2a$ site, of the Na/Cs atoms at the $6d$ site, and of all the Zn/Ge atoms, respectively.
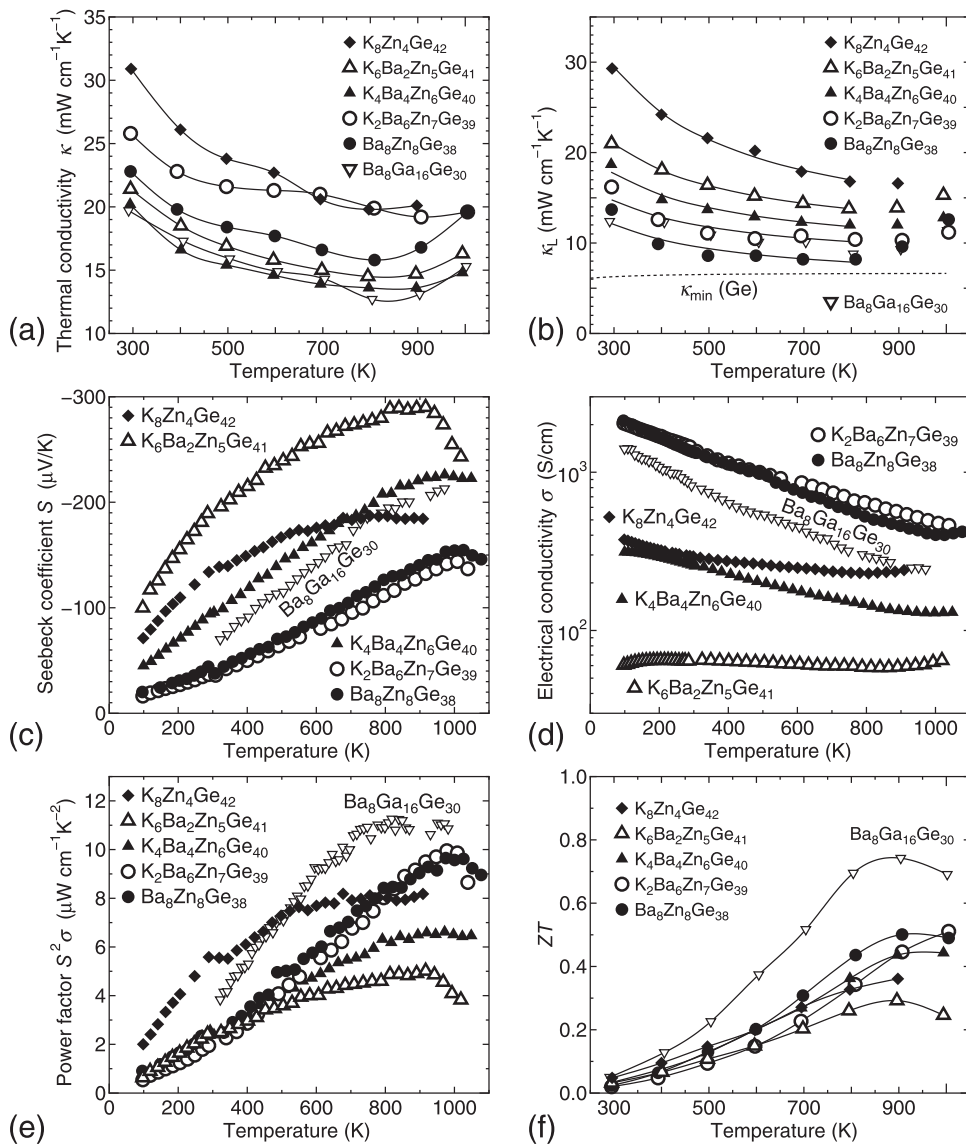
FIG. 8. Temperature dependences of (a) thermal conductivity $\kappa$, (b) lattice thermal conductivity $\kappa_L$, (c) Seebeck coefficient $S$, (d) electrical conductivity $\sigma$, (e) power factor $S^2\sigma$, and (f) dimensionless figure-of-merit $ZT$ for the $K_xBa_{8-x}Zn_{8-x/2}Ge_{38+x/2}$ and $Ba_8Ga_{16}Ge_{30}$ samples. The curves in (a) and (f) are guides for the eyes; the solid curves in (b) fit the relation $\kappa_L = K1 + K2/T$ ($K1$, $K2$: constant), and the dotted curve in (b) represents the theoretical minimum value $\kappa_{min}$ of Ge (Ref. 38).

phonon scattering. Consequently, we obtain $\mu_1 = \mu_{al} = M1$ and $\mu_2 = \mu_{ac} = M2/T$.

In contrast, substantial ordering of the atomic configuration and a decrease in the number of Zn atoms substituting for Ge in the framework were obtained for the K-containing $K_xBa_{8-x}Zn_yGe_{46-y}$ samples. Accordingly, alloy disorder scattering in the samples was expected to be suppressed. However, as mentioned above, the estimated mobilities $\mu_{al}$ dominated by alloy disorder scattering were 22.4 and 12.5 cm$^2$ V$^{-1}$ s$^{-1}$, respectively, for the samples with $x = 2$ and 4, which were smaller than that of 32.3 cm$^2$ V$^{-1}$ s$^{-1}$ for the sample with $x = 0$. We thus speculate that the alloy disorder scattering caused by the Zn/Ge atoms sitting in the framework would have weakened, whereas other alloy disorder scattering, as a result of the combination of K and Ba atoms sitting in the clathrate cage, might have strengthened. Figure 3 implies that the conduction band minima for the $K_xBa_{8-x}Zn_yGe_{46-y}$ samples differ in the areas around the rattler K and Ba atoms; we believe that the difference strengthened the scattering as a result of mixing of the K and Ba atoms. In addition, the substitution of K for Ba increased

the effective mass, as seen before, which probably increased the alloy disorder scattering, because it is proportional to $m^{*5/2}$ (See Eq. (4)).

We performed additional band structure calculations for hypothetical clathrates containing other alkali metals instead of K. Figure 7 shows the band structures and DOSs for the hypothetical clathrates $Na_8Zn_4Ge_{42}$ and $Cs_8Zn_4Ge_{42}$ (Ref. 36). The band gap energy for $Na_8Zn_4Ge_{42}$ is closer to that for $Ba_8Zn_8Ge_{38}$ than to that for $K_8Zn_4Ge_{42}$. Alloy disorder scattering is considered to strengthen with band edge discontinuities or band gap differences.[37] Consequently, increases in mobility for the $Na_xBa_{8-x}Zn_yGe_{46-y}$ clathrate might be expected to be caused by suppression of alloy disorder scattering.

The samples with higher K contents all possessed larger effective masses and reduced mobilities, although the $K_8Zn_4Ge_{42}$ sample had a larger mobility than that of the $K_6Ba_2Zn_5Ge_{41}$ sample. The reason is that the former sample did not suffer from alloy disorder scattering caused by mixing of the K and Ba atoms; its temperature-dependent mobility (Fig. 6(b)) has hardly any $T^0$ contribution caused by alloy disorder scattering.

## C. Thermoelectric properties

Figure 8 plots the temperature dependences of thermal conductivities $\kappa$, lattice thermal conductivities $\kappa_L$, the Seebeck coefficients $S$, electrical conductivities $\sigma$, the power factors $S^2\sigma$, and the dimensionless figures-of-merit $ZT$ for the $K_xBa_{8-x}Zn_{8-x/2}Ge_{38+x/2}$ and $Ba_8Ga_{16}Ge_{30}$ samples.

All the lattice thermal conductivity values decreased with temperature below 800 K (Fig. 8(b)); some of them increased with temperature above 800 K because of intrinsic conduction. The solid curves fit the relation $\kappa_L = K_1 + K_2/T$, where $K_1$ and $K_2$ are constants. The results are as follows: ($K1$ (mW cm$^{-1}$ K$^{-1}$), $K2$ (mW/cm)) = (5.4, 2000), (7.4, 2200), (8.3, 2800), (9.5, 3400), and (9.5, 6000) for $x = 0$, 2, 4, 6, and 8, respectively. The term $K_2/T$ represents the decrease caused by phonon-phonon scattering. Such decreases are clearly seen for all the samples, which indicates that rattling did not completely suppress thermal conduction in the $(K,Ba)_8(Zn,Ge)_{46}$ system at low temperatures. The RT $\kappa_L$ value of 14 mW cm$^{-1}$ K$^{-1}$ for $Ba_8Zn_8Ge_{38}$ was approximately equal to that previously reported.[22] The dotted curve represents the theoretical minimum value $\kappa_{min}$ for Ge.[38] The value for $Ba_8Zn_8Ge_{38}$ became close to the $\kappa_{min}$ value at high temperatures as a result of rattling and phonon-phonon scattering.

In contrast, the $K1$ values for the $K_x Ba_{8-x} Zn_{8-x/2} Ge_{38+x/2}$ samples increased with the K content $x$; their $\kappa_L$ values were not small enough. As seen above, the samples with higher K contents had larger equivalent atomic displacement parameters $U_{eq}$ as well as smaller split distances $d$. A large $U_{eq}$ value decreases the thermal conductivity, whereas a small $d$ value does not decrease it.[31,32] In addition, the samples with higher K contents had lighter average atomic weights of the rattler K/Ba atoms; this did not promote a reduction in thermal conductivity.

The temperature dependences of the Seebeck coefficients $S$ and electrical conductivities $\sigma$ (Figs. 8(c) and 8(d)) show typical behaviors of $n$-type degenerate semiconductors. The power factor $S^2\sigma$ reached 10 $\mu$W cm$^{-1}$ K$^{-2}$ at around 1000 K for the $K_2Ba_6Zn_7Ge_{39}$ sample. At low temperatures, around RT, the $S^2\sigma$ value of the $K_8Zn_4Ge_{42}$ sample was larger than those of the other samples, including that of the $Ba_8Ga_{16}Ge_{30}$ sample; this is a result of its larger weighted mobility (Table II). Similar data were obtained for the Ni-substituted Ge clathrates.[8] The maximum $ZT$ value obtained in this study was 0.51 at 1000 K for the $K_2Ba_6Zn_7Ge_{39}$ sample; unfortunately, this is substantially lower than that of the $Ba_8Ga_{16}Ge_{30}$ sample.

## IV. CONCLUSIONS

We prepared several polycrystalline samples of $n$-type clathrate $K_xBa_{8-x}Zn_yGe_{46-y}$ ($y \sim 8 - x/2$), whose Zn atoms preferred to exist at the $6c$ sites in the framework. The clathrate samples with $x$ around 4, such as $K_4Ba_4Zn_6Ge_{40}$, had smaller numbers of substituting Zn atoms, as well as more ordered Zn/Ge atom frameworks, than the $Ba_8Zn_8Ge_{38}$ sample did. However, the former exhibited lower carrier mobilities, contrary to expectations. This is probably associated with the influences of mixing of the K and Ba atoms in the cages on the conduction band edge. Band structure calculations suggest that the mixing would have strengthened alloy disorder scattering. The calculations also imply that we could possibly obtain increased mobility for a clathrate $Na_4Ba_4Zn_6Ge_{40}$. However, since influences on the valence band edge seem to be almost absent, we expect that the carrier mobility might be improved in $p$-type $K_xBa_{8-x}Zn_yGe_{46-y}$ clathrates.

[1]See, for example, H. J. Goldsmid, *Electronic Refrigeration* (Pion, London, 1986), Chaps. 2–3, pp. 17–87.

[2]G. S. Nolas, J. L. Cohn, G. A. Slack, and S. B. Schujman, Appl. Phys. Lett. **73**, 178 (1998).

[3]V. L. Kuznetsov, L. A. Kuznetsova, A. E. Kaliazin, and D. M. Rowe, J. Appl. Phys. **87**, 7871 (2000).

[4]G. S. Nolas, G. A. Slack, and S. B. Schujman, in *Recent Trends in Thermoelectric Materials Research I*, edited by T. M. Tritt (Academic, San Diego, 2001), chap. 6, pp. 255–300.

[5]P. Rogl, in *Thermoelectrics Handbook: Macro to Nano*, edited by D. M. Rowe (CRC, Boca Raton, FL, 2006), chap. 32, pp. 32-1–32-24.

[6]A. V. Shevelkov and K. Kovnir, in *Zintl Phases: Principles and Recent Developments*, edited by T. F. Fässler (Springer, Berlin, 2011), pp. 97–142.

[7]A. Saramat, G. Svensson, A. E. C. Palmqvista, C. Stiewe, E. Mueller, D. Platzek, S. G. K. Williams, D. M. Rowe, J. D. Bryan, and G. D. Stucky, J. Appl. Phys. **99**, 023708 (2006).

[8]X. Shi, J. Yang, S. Bai, J. Yang, H. Wang, M. Chi, J. R. Salvador, W. Zhang, L. Chen, and W. Wong-Ng, Adv. Funct. Mater. **20**, 755 (2010).

[9]N. L. Okamoto, K. Kishida, K. Tanaka, and H. Inui, J. Appl. Phys. **101**, 113525 (2007).

[10]K. Momma and F. Izumi, J. Appl. Crystallogr. **44**, 1272 (2011).

[11]J. Martin, H. Wang, and G. S. Nolas, Appl. Phys. Lett. **92**, 222110 (2008).

[12]B. C. Sales, B. C. Chakoumakos, R. Jin, J. R. Thompson, and D. Mandrus, Phys. Rev. B **63**, 245113 (2001).

[13]M. Hokazono, H. Anno, and K. Matsubara, Mater. Trans. **46**, 1485 (2005).

[14]E. Alleno, G. Maillet, O. Rouleau, E. Leroy, C. Godart, W. Carrillo-Cabrera, P. Simon, and Yu. Grin, Chem. Mater. **21**, 1485 (2009).

[15]M. Hayashi, K. Kishimoto, K. Kishio, K. Akai, H. Asada, and T. Koyanagi, Dalton Trans. **39**, 1113 (2010).

[16]Q. Xie, Ph.D. dissertation, Swiss Federal Institute of Technology Zurich, 2004.

[17]S. Anno, K. Kishimoto, and T. Koyanagi, in *Proceedings of 2nd Meeting of the Thermoelectrics Society of Japan, 2005*, pp. 46–47.

[18]G. Cordier and P. Woll, J. Less-Common Met. **169**, 291 (1991).

[19]S. Johnsen, A. Bentien, G. K. H. Madsen, B. B. Iversen, and M. Nygren, Chem. Mater. **18**, 4633 (2006).

[20]S. Johnsen, A. Bentien, G. K. H. Madsen, M. Nygren, and B. B. Iversen, Phys. Rev. B **76**, 245126 (2007).

[21]N. Melnychenko-Koblyuk, A. Grytsiv, L. Fornasari, H. Kaldarar, H. Michor, F. Röuhrbacher, M. Koza, E. Royanian, E. Bauer, P. Rogl, M. Rotter, H. Schmid, F. Marabelli, A. Devishvili, M. Doerr, and G. Giester, J. Phys.: Condens. Matter **19**, 216223 (2007).

[22]M. Christensen and B. B. Iversen, J. Phys.: Condens. Matter **20**, 104244 (2008).

[23]M. Christensen, S. Johnsen, F. Juranyi, and B. B. Iversen, J. Appl. Phys. **105**, 073508 (2009).

[24]M. M. Koza, M. R. Johnson, H. Mutka, M. Rotter, N. Nasir, A. Grysiv, and P. Rogl, Phys. Rev. B **82**, 214301 (2010).

[25] N. Nasir, A. Grytsiv, N. Melnychenko-Koblyuk, P. Rogl, I. Bednar, and E. Bauer, J. Solid State Chem. **183**, 2329 (2010).

[26] L. T. K. Nguyen, U. Aydemir, M. Baitinger, E. Bauer, H. Borrmann, U. Burkhardt, J. Custers, A. Haghighirad, R. Höfler, K. D. Luther, F. Ritter, W. Assmus, Yu. Grin, and S. Paschen, Dalton Trans. **39**, 1071 (2010).

[27] K. Ohoyama, T. Kanouchi, K. Nemoto, M. Ohashi, T. Kajitani, and Y. Yamaguchi, Jpn. J. Appl. Phys., Part 1 **37**, 3319 (1998).

[28] F. Izumi and K. Momma, Solid State Phenom. **130**, 15 (2007).

[29] P. Blaha, K. Schwarz, G. Madsen, D. Kvasnicka, and J. Luitz, Program package WIEN2K, Technical University of Vienna, 2001.

[30] J. P. Perdew, K. Burke, and M. Ernzerhof, Phys. Rev. Lett. **77**, 3865 (1996).

[31] N. L. Okamoto, J. Kim, K. Tanaka, and H. Inui, Acta Mater. **54**, 5519 (2006).

[32] B. C. Chakoumakos, B. C. Sales, D. G. Mandrus, and G. S. Nolas, J. Alloys Compd. **296**, 80 (2000).

[33] For $Ba_8Zn_8Ge_{38}$, the virtual atomic numbers of the virtual Zn/Ge atoms at the $6c$, $16i$, and $24k$ sites were set to be 30.23, 31.91, and 31.83, respectively; for that of $K_8Zn_4Ge_{42}$, the virtual Zn/Ge atoms at the $6c$ site was set to be 30.67, while the atomic numbers of the Ge atoms at the $16i$ and $24k$ sites were 32.

[34] T. Eto, K. Kishimoto, K. Koga, K. Akai, T. Koyanagi, H. Anno, T. Tanaka, H. Kurisu, S. Yamamoto, and M. Matsuura, Mater. Trans. **50**, 631 (2009).

[35] A. Bentien, V. Pacheco, S. Paschen, Yu. Grin, and F. Steglich, Phys. Rev. B **71**, 165206 (2005).

[36] The two hypothetical clathrates' atomic coordinations were set to be equal to those of the $K_8Zn_4Ge_{42}$ sample, while their lattice constants were optimized in band structure calculations.

[37] S. Krishnamurthy, A. Sher, and A.-B. Chen, Appl. Phys. Lett. **47**, 160 (1985).

[38] D. G. Cahill, S. K. Watson, and R. O. Pohl, Phys. Rev. B **46**, 6131 (1992).